The Coalescence of Drops in Liquid-Liquid Fluidized Beds

MARIO J. MARASCHINO and ROBERT E. TREYBAL

New York University, New York, New York

The coalescence rates of equisized drops of organic liquids fluidized by water under conditions of mutual saturation were studied. A drop-size separation technique permitted the direct count of the coalesced drops. Six organic liquids (benzene, cyclohexane, *n*-butylacetate, methyl isobutyl ketone, diisobutyl carbinol, and tetrahydrobenzaldehyde) were used, and the coalescence was in all cases total, that is, without formation of small satellite drops.

A new hydrodynamic model is presented to calculate the parameters governing the drainage of liquid between two deformable drops in head-on collision. A parameter from this model permits correlation of the coalescence rates with only two arbitrary constants, provided the ratio of dispersed to continuous liquid viscosities lies between 0.5 and 2. High viscosity ratios or the presence of trace quantities of surfactant greatly depress the coalescence rate, while continued reuse of the dispersed liquid leads to a statistically significant reduction. The presence of a fog of very small droplets increases the coalescence rate.

In recent years evidence has been accumulating that the coalescence of drops in a liquid-liquid dispersion has a strong influence on the performance of liquid-extraction devices. For example, coalescence has been shown to be detrimental to the performance of spray towers (*1*). On the other hand, coalescence and redispersion of the drops in an agitated vessel are suspected of being responsible for enhanced mass transfer rates (*20*).

The coalescence phenomenon is poorly understood. The extensive work on the time of coalescence of single drops at a flat interface, recently reviewed (*4*, *14*), has resulted in only one proposed correlation (*13*), which is totally empirical and involves many arbitrary constants. Quantitative studies for multiple-drop systems have been confined to agitated vessels (*8*, *10*, *13*, *17*, *18*). The techniques used usually involved some type of drop tracer study requiring an indirect method of observation and contamination of the liquid system with a tracer. This makes interpretation of the results difficult, since the coalescence phenomenon is extremely sensitive to contaminants. The only correlation relating coalescence rate to all physical properties is that of Hillestad and Rushton (*10*), which uses many arbitrary constants. Only qualitative information is available for spray towers (*7*, *15*).

In the present study, the coalescence rates for a swarm of uniformly sized drops maintained in a fluidized bed were studied. A drop-size segregation technique was used, so that newly formed coalesced drops were quickly removed from the bed, at a rate determined by direct counting. It is believed that the conditions of measurement exerted a minimal influence on the phenomenon.

APPARATUS AND PROCEDURE

The vertical glass tube of Figure 1 consists of two tubes of uniform but different diameters joined by a tapered section. The continuous liquid enters from the top and flows downward. The dispersed phase, consisting of uniform, small drops, enters at the bottom and rises. It is possible to adjust the continuous phase flow rate so that the small drops just barely do not escape out of the narrow section. This will be referred to as the critical filter condition.

Mario J. Maraschino is with Halcon International Inc., New York, New York.

At the critical filter condition, the entering drops will accumulate in and below the taper to form a fluidized bed of drops. If two drops in the bed coalesce to form a large drop, and if both sizes are below a certain critical size (*21*), the large drop which rises faster will escape from the bed, pass through the narrow section, and leave at the top.

The tube of Figure 1 was mounted inside a stainless steel tank with glass windows at the front and back for unhindered visibility, as in Figure 2. The spray head at the bottom contained 24 nozzles of stainless steel tubing 0.010 in. I.D., 0.020 in. O.D. The nozzle tips were chamferred at 45 deg. so that the issuing drops formed at the smaller diameter. At the top, a section of 1-in. Pyrex pipe served as a collection device to measure accumulated dispersed phase.

Two glass tubes were used: for the first $D_n = 2.355$ in., $D_w = 2.570$ in., $L = 0.892$ in.; for the second $D_n = 2.155$ in., $D_w = 2.555$ in., $L = 1.497$ in. The tube with the larger value of D_w/D_n resulted in a larger dispersed phase fraction in the fluidized bed at the critical filter condition.

Before a run was begun, the drop size was determined for the prevailing conditions by measurement of the collected volume of a known number of drops. With the continuous liquid flowing at the critical filter condition, the bed of drops was then established. If the coalescence rate was large ($w > 0.1$ min.$^{-1}$), the equipment was operated in a continuous manner, that is, the rate of dispersed phase entering the bed equaled that which left the bed at steady state. If the coalescence rate was small ($w < 0.03$ min.$^{-1}$), a batch procedure was used: dispersed phase flow was stopped. The height of the fluidized bed and the time rate of leaving dispersed phase (both by drop count and accumulation in the collection tube) were recorded. At the end of the run, the bed holdup of dispersed phase was determined by draining the bed contents into the collection tube. The run was repeated many times, and the coalescence rates averaged. Further details are available elsewhere (*16*).

Six organic liquids—benzene, cyclohexane, *n*-butyl acetate (BuOAc), methyl isobutyl ketone (MIBK), diisobutyl carbinol (DBC), and 1, 2, 3, 6-tetrahydrobenzaldehyde (THB)—were studied as the dispersed phase with water continuous, both phases mutually saturated. The ranges of physical properties were $\sigma = 10.0$ to 47.8 dynes/cm., $\rho_c = 0.9960$ to 0.9998 g./cu. cm., $\rho_d = 0.7735$ to 0.9756 g./cu. cm., $\Delta\rho = 0.0242$ to 0.2235 g./cu. cm., $\mu_c = 0.862$ to 1.096 centipoise, $\mu_d = 0.596$ to 8.475 centipoise.

EXPERIMENTAL RESULTS

The data are presented in Table 1. The coalescence of equisized drops was to a large extent complete. Fragmentary, small drops were very seldom observed. The fractional coalescence rate w is defined as

$$w = Q/N \qquad (1)$$

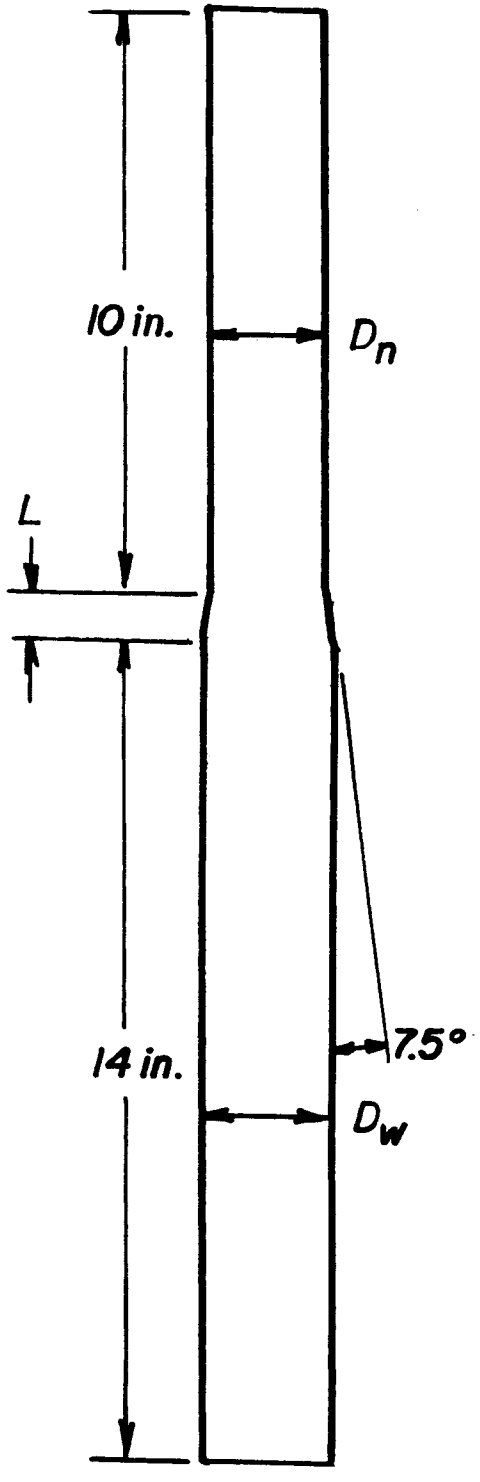

Fig. 1. Schematic diagram of glass tube.

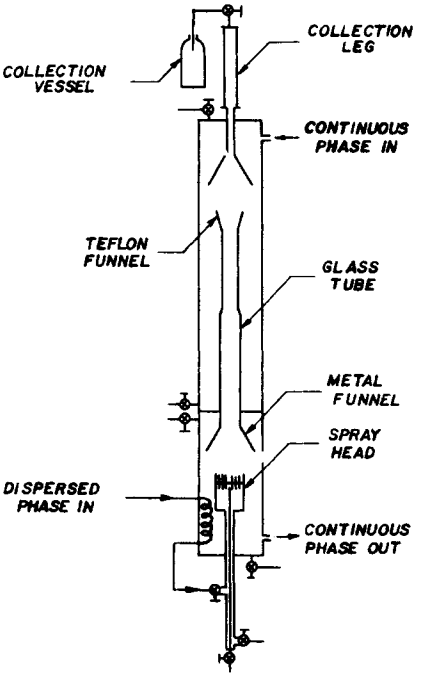

Fig. 2. Schematic arrangement of apparatus.

w^{-1} represents the average time that a drop remains in the bed before being removed by coalescence. In terms of the coalesced drops leaving the bed

$$w = 2\ (\text{drop-leaving rate})/N \tag{2}$$

The volume of collected drop liquid and the drop count indicated that occasionally a large drop resulting from a two-drop coalescence would coalesce with a small drop before being completely removed from the bed. Nevertheless, by virtue of the method of measurement, w represents only the original coalescence of two drops of small size. It was found to be independent of bed depth.

Dimensional analysis indicates that w may be related to the fluid properties and bed characteristics through the following dimensionless groups: wD/V_s, $N_{Re} = DV_s\rho_c/\mu_c$, $N_{Co} = \sigma g_c/\mu_c V_s$, ϕ_d, $\Delta\rho/\rho_c$, μ_d/μ_c. The following development is an analytical approach to obtain the relationship.

COLLISION THEORY

For multiparticle systems, the coalescence frequency may be considered as the product of the collision frequency for the particles and the fraction n of collisions resulting in successful coalescence (*11*). If t_c is the average time

Table 1. System Properties and Coalescence Rates

Dispersed liquid	μ_c, centipoise	μ_d, centipoise	ρ_c, g./cu. cm.	ρ_d, g./cu. cm.	σ, dynes/cm.	D, cm.	ϕ_d	V_s, cm./sec.	w, min.$^{-1}$	Std. dev. of mean for w, %
Benzene	0.948	0.613	0.9980	0.8750	32.1	0.355	0.0373	7.27	0.503	5.0
Cyclohexane	0.874	0.860	0.9970	0.7735	47.8	0.312	0.0373	10.37	1.503	5.0
BuOAc	0.967	0.711	0.9984	0.8802	13.5	0.267	0.0298	7.15	0.0269	5.6
	0.976	0.764	0.9985	0.8805	13.4	0.261	0.0582	6.21	0.1129	4.3
MIBK	1.016	0.596	0.9960	0.8035	10.0	0.198	0.0472	7.19	0.1297	3.6
	1.015	0.596	0.9960	0.8035	10.05	0.201	0.0236	8.37	0.0116	7.0
DBC	0.862	8.450	0.9964	0.8082	16.8	0.244	0.0302	7.55	0.00226	4.4
	0.862	8.475	0.9964	0.8082	16.9	0.244	0.0598	6.65	0.00250	9.2
THB	1.096	1.989	0.9998	0.9756	12.6	0.446	0.0647	2.68	0.1468	1.2
Benzene + surfactant	0.957	0.626	0.9977	0.8754	29.1	0.334	0.0328	6.88	0.00302	11.3

between collisions for a drop, then

$$n = wt_C \tag{3}$$

Howarth (*11*) developed an expression for the time between collisions:

$$\frac{1}{t_C} = \left[\frac{24R\overline{u^2(t)}\phi_d}{D^3}\right]^{0.5} \tag{4}$$

Then

$$n = \left(\frac{D}{24R}\right)^{0.5} \frac{wD}{[\overline{u^2(t)}\phi_d]^{0.5}} \tag{5}$$

With the assumption that the fluctuating velocity $[\overline{u^2(t)}]^{0.5}$ is proportional to the slip velocity V_s, then

$$\frac{n}{\text{constant}} = \bar{n} = \frac{wD/V_s}{\phi_d^{0.5}} \tag{6}$$

where

$$V_s = \frac{V_c}{1-\phi_d} + \frac{V_d}{\phi_d} \tag{7}$$

The dimensionless quantity $\bar{n}$, which is proportional to the fraction of successful collisions, can be calculated directly from the experimental data.

It seems reasonable that the closer two drops are capable of approaching each other, the greater should be the probability of their coalescence. It is conceivable that $\bar{n}$ may be representable as some function of a parameter representing the drainage of intervening continuous phase liquid. To test this hypothesis, a means of calculating the minimum film thickness between two deformable drops is needed. The only previous work is a theoretical investigation of head-on collision of two equisized drops by Damon (*6*), who used a totally numerical procedure. His results are questionable for two reasons: his solution did not converge when higher order polynomial approximations were used; and the model predicts that the drops can physically touch each other, whereas from Equation (15) it would appear that this is impossible. The following new approach was developed.

DROP COLLISION MODEL

Consider two equisized drops approaching one another along the z axis (Figure 3*a*). Let the origin be located midway between the drops. For convenience the top drop can be analyzed separately as it approaches the plane of symmetry. The mechanism for the drop approach is divided into two stages. In the first stage, the drop is assumed to behave as a rigid sphere. For the initial position $H = H_o$, the top drop moves downward, eventually reaching a position H_i where it becomes impossible for the drop to remain spherical. This transition is taken to occur where the pressure at the apex of the drop equals its internal pressure. A deformation mechanism (second stage) now begins, during which the drop deforms in an elastic manner as the film of intervening liquid simultaneously drains. During the second stage the instantaneous shape of the drop is assumed to be that of a truncated sphere (Figure 3*b*). This shape is used because it minimizes the instantaneous surface (potential) energy of the drop (*16*). The equations for the two stages are derived below, and in greater detail elsewhere (*16*). They show that all collision parameters are completely determined if $\bar{N}_{Re} = DV_o\rho_d/\mu_c$, $\bar{N}_{Co} = \sigma_{g_c}/\mu_c V_o$, and H_o/D are specified.

Generalized Film Drainage

The derivation will be performed in cylindrical coordinates (Figure 4). Consider a drainage profile $h = h(r)$ of some arbitrary shape (Figure 5). For an incompressible fluid, neglect of inertial terms, symmetry with respect to the z axis, and the approaching profiles in close proximity, the Navier-Stokes equation (*2*, *16*) and the viscous dissipation equation (*2*, *5*, *16*) take the following forms, respectively:

$$\frac{g_c}{\mu_c}\frac{\partial p}{\partial r} = \frac{\partial^2 v_r}{\partial z^2} \tag{8}$$

$$\tau : \nabla \mathbf{v} = \left(\frac{\partial v_r}{\partial z}\right)^2 \tag{9}$$

It is common to assume a parabolic velocity profile for a draining film (*5*):

$$v_r = \frac{3V_r}{4h^3}(h^2 - z^2) \tag{10}$$

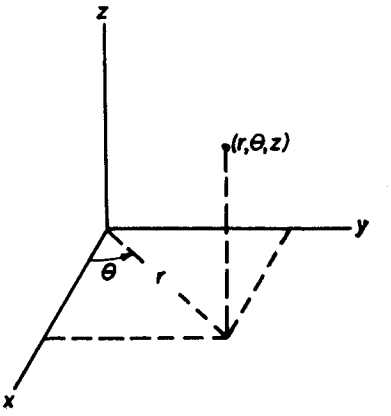

Fig. 4. Coordinate system.

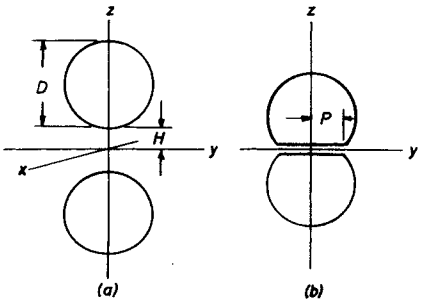

Fig. 3. Colliding drops.

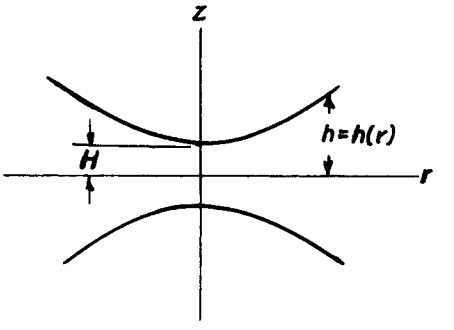

Fig. 5. Drainage profile.

The rate at which energy enters the draining film must equal that at which energy is dissipated in the film:

$$FV = \iiint (\tau : \nabla \mathbf{v}) r\, dr\, d\theta\, dz \tag{11}$$

Substitution of Equation (10) into Equation (9) and integration result in

$$F = \frac{3\pi\mu_c V}{2g_c} \int_0^{r_m} \frac{r^3}{h^3} dr \tag{12}$$

First Stage

For an approaching sphere, the parabolic approximation to a sphere, $h = H + r^2/D$, is substituted into Equation (11). Integration from $r = 0$ to $r = D/2$ and the assumption $H/D < 0.25$ result in

$$F_s = \frac{3\pi\mu_c V}{8g_c H^3} (DH)^2 \tag{13}$$

Newton's second law is

$$F_s = \frac{m}{g_c} \frac{d^2H}{dt^2} \tag{14}$$

Substitution of Equation (13) into Equation (14), replacement of V by $-dH/dt$, and integration from H_o to H_i and from V_o to V_i, result in

$$\frac{V_i}{V_o} = 1 + \frac{9 \ln (H_i/H_o)}{4\bar{N}_{Re}} \tag{15}$$

Transition

The pressure difference between the inside and outside of a drop is given by the Laplace equation (9), which, for a sphere, is

$$\Delta p = 4\sigma/D \tag{16}$$

Substitution of Equation (10) into Equation (8), together with the parabolic approximation to a sphere, integration from $r = 0$ to $r = D/2$, and the further assumption that $H/D < 0.25$ result in

$$\Delta p = \frac{3\mu_c V D}{8g_c H^2} \tag{17}$$

Elimination of Δp between Equations (16) and (17) results in

$$\frac{H_i}{D} = \left(\frac{3}{32} \frac{V_i}{V_o \bar{N}_{Co}}\right)^{0.5} \tag{18}$$

Deformation

The momentum of a drop can be computed as if the entire mass is located at the center of gravity. If the film between drops is thin, the momentum of the top drop can be dealt with as if the drops were touching. Refer to Figure 6, where C is the center of gravity. Newton's law is

$$F = \frac{m}{g_c} \frac{d^2S}{dt^2} \tag{19}$$

Letting $\psi = 1 - 2S/D$, and replacing S by ψ through the chain rule

$$F = \frac{-mD}{2g_c} \frac{d^2\psi}{dt^2} \tag{20}$$

The only potential energy of the drop is that stored in its surface area, which is a function of the drop shape, in turn a function of S. Thus $E_p = E_p(S)$. The assumption of an elastic collision requires the potential energy field to be

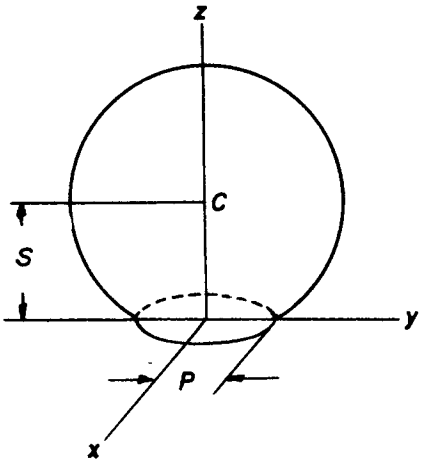

Fig. 6. Drop parameters.

conservative. Thus

$$F = -\partial E_p/\partial S \tag{21}$$

In terms of ψ, this becomes

$$F = \frac{2}{D} \frac{\partial E_p}{\partial \psi} \tag{22}$$

The total surface area of the drop can be represented in terms of ψ (16):

$$A = \pi D^2(1 + \psi^2/4 + \psi^3/3 + 3\psi^4/16 + \cdots) \tag{23}$$

With $E_p = \sigma A$, substitution of Equation (23) into Equation (22) results in

$$F = \sigma\pi D(\psi + 2\psi^2 + 3\psi^3/2 + \cdots) \tag{24}$$

With $F = F(\psi)$, Equation (20) may be integrated subject to the initial conditions $S = D/2$ and $dS/dt = -V_i$, or, in terms of $\psi = \psi(t)$, $\psi(0) = 0$ and $d\psi(0)/dt = 2V_i/D$. Substitution of a one-term approximation of Equation (24) into Equation (20) and integration result in

$$\psi = \left(\frac{4E_K}{\pi\sigma D^2}\right)^{0.5} \sin\left[\left(\frac{2\pi\sigma g_c}{m}\right)^{0.5} t\right] \tag{25}$$

Equations (24) and (25) result in

$$F = (4\pi E_K \sigma)^{0.5} \sin\left[\left(\frac{2\pi\sigma g_c}{m}\right)^{0.5} t\right] \tag{26}$$

From geometric considerations, it can be shown (16) that

$$(P/D)^2 = \psi/2 + \psi^2/4 + \cdots \tag{27}$$

Substitution of Equation (25) into Equation (27 results in

$$\left(\frac{P}{D}\right)^2 = \left(\frac{E_K}{\pi\sigma D^2}\right)^{0.5} \sin\left[\left(\frac{2\pi\sigma g_c}{m}\right)^{0.5} t\right] \tag{28}$$

The time necessary for the drop to reach maximum deformation occurs when $d\psi/dt = 0$. This provides

$$t_m = \left(\frac{\pi m}{8\sigma g_c}\right)^{0.5} \tag{29}$$

The profile of a deformed drop, Figure 7, may be substituted into Equation (12). The profile $h = H$ is used for the integration from $r = 0$ to $r = P$. The profile $h = h_S + r^2/D$, where $h_S = H - P^2/S$, is used for the integration from $r = P$ to $r = D/2$. With the assumption $H/D < 0.25$,

$$F_t = \frac{3\pi\mu_c V}{8g_c H^3} (P^4 + HDP^2 + H^2D^2) \tag{30}$$

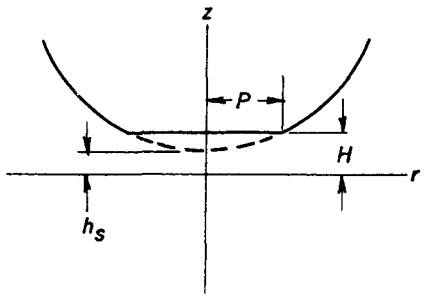

Fig. 7. Distorted drop.

In Damon's numerical analysis (6), the approach of a drop was considered to take place as a series of finite incremental steps. Each increment had a fixed, rigid drop profile, and the profile was corrected between increments. The following procedure is analytical, where the increments are differential rather than finite.

In Equation (30), let $V = -dH/dt$ and substitute F [Equation (26)] and P [Equation (28)]. Introduction of the working variables M and Ω results in the following:

$$M = (H/D)^{-2} \tag{31}$$

$$\Omega = -\cos\left[\left(\frac{2\pi\sigma g_c}{m}\right)^{0.5} t\right] \tag{32}$$

$$\bar{P}_m^4 = \bar{N}_{Re}\,(V_i/V_o)/12\bar{N}_{Co} \tag{33}$$

$$\frac{dM}{d\Omega} = \frac{32\bar{N}_{Co}}{3(V_i/V_o)\{1-\Omega^2+[(1-\Omega^2)/(\bar{P}_m^4 M)]^{0.5}+1/\bar{P}_m^4 M\}} \tag{34}$$

The initial condition is $H = H_i$. Integration from $\Omega = -1$ to 0 produces $H = H_m$, the film half-thickness at maximum drop deformation ($t = t_m$). Integration from $\Omega = 0$ to 1 produces $H = H_f$, the film half-thickness at the end of the deformation process ($t = 2t_m$). After this, the drops separate.

To summarize, in the first stage the drops maintain their spherical shape and are described by Equation (15). In the second stage the drops deform, and are described by Equations (31) to (34). The transition between stages is given by Equation (18). Computations were performed for an array of values of $\bar{N}_{Re}$ and $\bar{N}_{Co}$, with $H_o/D = 0.125$; a Fortran program is available (*16*). The results are shown in Figures 8 and 9.

Restrictions

In order that $H_o > H_i$, it is necessary that

$$\bar{N}_{Re} > 9/8, \quad \bar{N}_{Co} > (3/32)/(H_o/D)^2 \tag{35}$$

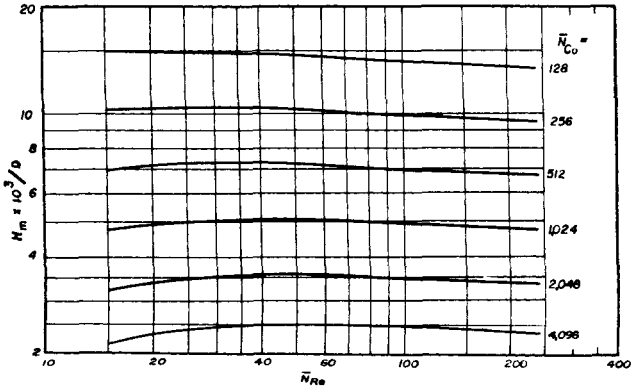

Fig. 8. Film drainage parameter H_m/D for $H_o/D = 0.125$.

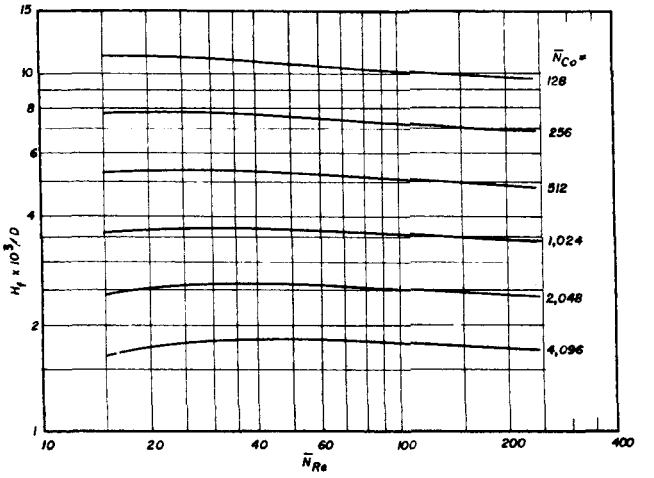

Fig. 9. Film drainage parameter H_f/D for $H_o/D = 0.125$.

In order to guarantee the absolute convergence of the power series used in the development, it is necessary that

$$\bar{P}_m = P_m/D \leq 0.707 \tag{36}$$

In order for Equation (25) to be valid, the distance that the center of gravity traverses due to drop-shape considerations $\psi_m D/2$ must be greater than that due to movement of the leading edge of the drop:

$$\psi_m >> H_i/D - H_m/D \tag{37}$$

where (*16*)

$$\psi = 2(P/D)^2 - 2(P/D)^4 + 2(P/D)^6/3 + \cdots \tag{38}$$

In order for deformation to occur, the drop must not be too rigid (*16*):

$$\bar{N}_{Co} < 3[32B(H_o/D)^2 \exp(1-B)]^{-1} \tag{39}$$

where $B = 8\bar{N}_{Re}/9$. If the drops are too rigid, they follow Equation (15) with $V_i/V_o = 0$.

CORRELATION

It was suggested earlier that $\bar{n}$ should be an unique function of some film thickness parameter, such as H_m/D or H_f/D. To test this hypothesis, the center-to-center collision velocity $2V_o$ was set arbitrarily at various fractions of the slip velocity V_s, and H_m/D and H_f/D were computed for each run. At $2V_o = V_s/4$, corresponding to $\bar{N}_{Re} = N'_{Re}/8$ and $\bar{N}_{Co} = 8N_{Co}$, the best correlation was obtained.

In Figure 10 the circled points represent the results for all the binary systems for which μ_d/μ_c was between 0.5 and 2.0. The least-square line is

$$\log(\bar{n} \times 10^6) = 4.988 - 0.655(H_m \times 10^3)/D \tag{40}$$

In Figure 11 the least-square line is

$$\log(\bar{n} \times 10^6) = 4.959 - 0.874(H_f \times 10^3)/D \tag{41}$$

The correlation coefficient (*19*) in both cases is 0.94, and both correlations represent the data equally well. For the relatively low values of ϕ_d studied, with the understanding that μ_C was varied only minimally, and with the exceptions described below, the hypothesis seems verified.

HIGH VISCOSITY RATIO

On Figure 12 the triangle points represent the results for two groups of runs with diisobutyl carbinol, $\mu_d/\mu_c = 9.8$, as

the dispersed phase. The parameter $\bar{n}$ is smaller than that given by the general correlation by factors of 70 to 110. The alcohol also exhibited delayed coalescence in a simple shake-out test. Shaking the alcohol with water in a flask produced a fine alcohol dispersion which required about 1 hr. to settle out. Any other pure liquid pair with similar density difference and interfacial tension settled out in less than 1 min.

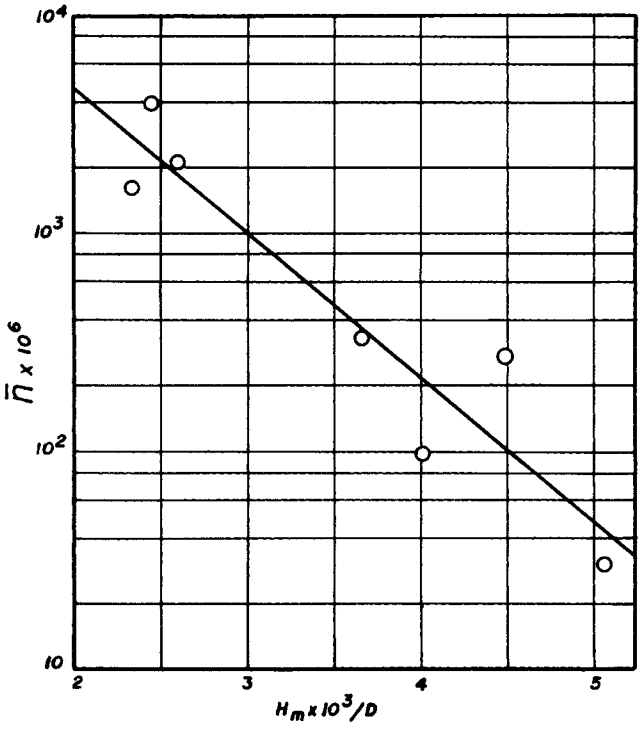

Fig. 10. Correlation of coalescence rate with H_m/D.

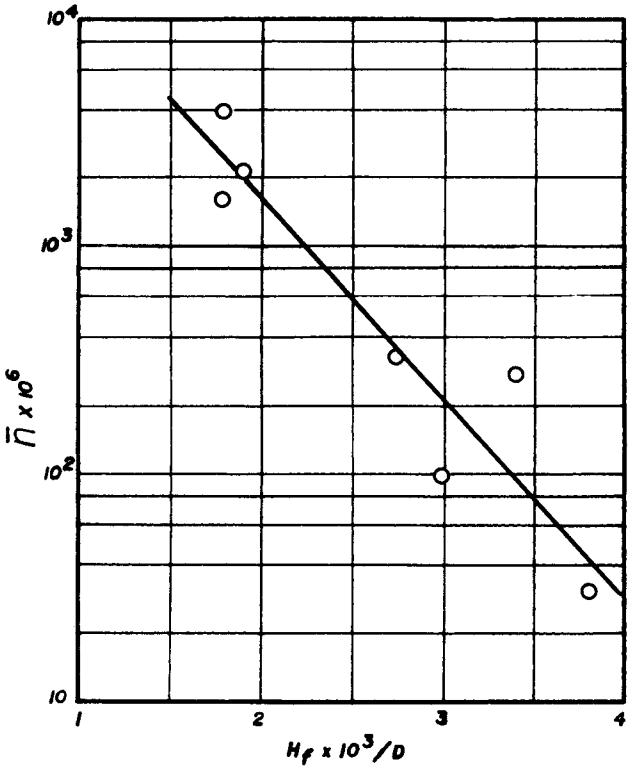

Fig. 11. Correlation of coalescence rate with H_f/D.

FINE DISPERSIONS

A series of consecutive measurements was taken with diisobutyl carbinol drops. Run A was taken under normal conditions. Before run B was carried out, a fine dispersion (fog) of alcohol microdrops was introduced into the continuous phase. Over a period of 5 hr., during which the fog gradually cleared, a dozen more runs were taken at uniform intervals with the usual size drops occupying the fluidized bed. The results are shown in Figure 13. A dense fog was considered one where the depth of visibility was greater than 4 in. but less than 8 in.

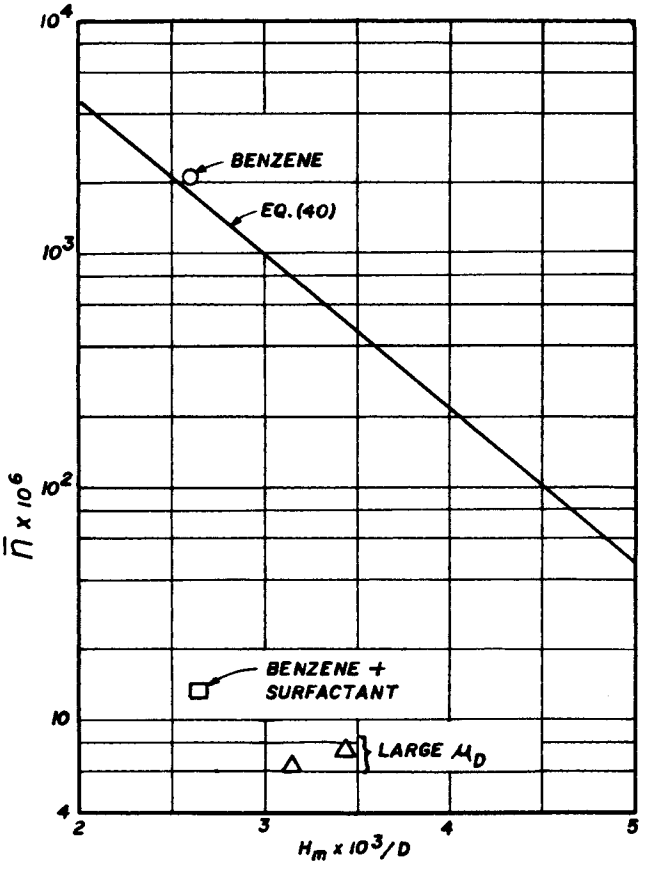

Fig. 12. Effect of high viscosity ratio and surfactant.

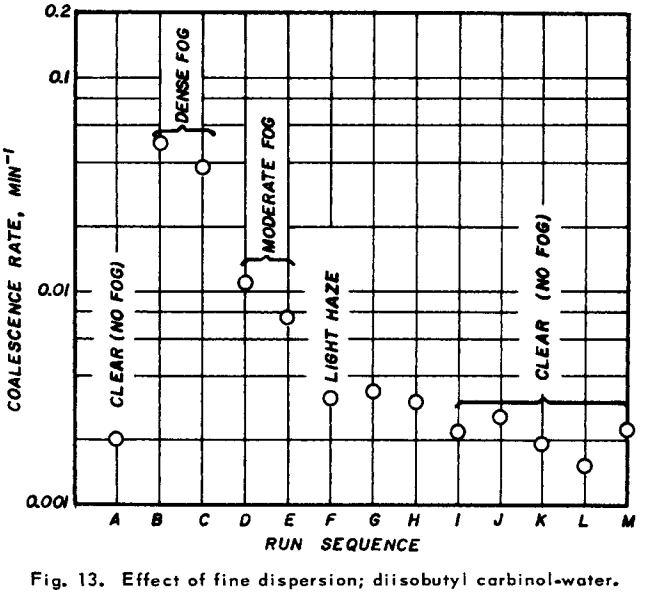

Fig. 13. Effect of fine dispersion; diisobutyl carbinol-water.

SURFACTANT

The benzene-water system was chosen to study the effect of a surfactant. The literature pertaining to the effect of surfactants on mass transfer in liquid-extraction operations reveals that the sodium salts of organic sulfates in the 11- to 16-carbon atom range (*3*) have profound influence at very low concentrations. The most readily available commercial material of this type was Tergitol No. 4, a salt of a 14-carbon organic sulfate diluted with water to 26 to 28% concentration.

The continuous phase consisted of 8.40 ml. of Tergitol No. 4 diluted with water to 50 gal., which provides a concentration of active surfactant of roughly 120 p.p.m. As shown in Figure 12, the coalescence rate of benzene (circled point) has been reduced 157-fold by the surfactant (square point). The corresponding reduction in interfacial tension was only 2.7 dynes/cm., which would normally result in an insignificant change in the coalescence rate.

RECYCLE

A group of three runs with benzene as the dispersed phase was taken. The benzene of the first run was reused for the second and again for the third. The coalescence rates were $w = 0.552$, 0.282, and 0.218 min.$^{-1}$, respectively. A second group of seven runs was taken without recycle of the benzene, and the average coalescence rate was 0.503 min.$^{-1}$, with a standard deviation of 0.067 min.$^{-1}$. Application of Student's t-distribution shows that the values of 0.282 and 0.218 min.$^{-1}$ represent a significant decrease in coalescence rate, exceeding the 5 and 1% level, respectively. Thus, recycling the organic liquid leads to a significant decrease in the coalescence rate.

Thus, Equations (40) and (41) represent the highest likely coalescence rates occurring only under conditions of extreme cleanliness and absence of surfactants, for uniform drop sizes, for relatively low volumetric fractions of dispersed phase, and in the absence of mass transfer. No reasons are now suggested for the observed deviations, which are the subject of continuing study.

ACKNOWLEDGMENT

We are grateful for the support of the National Aeronautics and Space Administration through a NASA Traineeship, and the American Chemical Society-Petroleum Research Fund.

NOTATION

A = surface area of drop, sq. cm.
D = diameter of drop, cm.
E_K = kinetic energy = $mV_i^2/2g_c$, ergs
E_P = potential energy, ergs
F = force, dynes
F_s = force on a sphere, dynes
F_t = force on a deformed sphere, dynes
g_c = conversion factor, (1 g.)(cm.)/(dyne)(sq. sec.)
H = minimum value for h, cm.
h = distance from a point on the drop surface to the plane $z = 0$, cm.
M = working variable, dimensionless
m = mass of drop, g.
N = number of drops in a fluidized bed, dimensionless
$\underline{N}_{Co}$ = coalescence number, $\sigma g_c/\mu_c V_s$, dimensionless
$\overline{N}_{Co}$ = coalescence number, $\sigma g_c/\mu_c V_o$, dimensionless
N_{Re} = Reynolds number, $DV_s \rho_c/\mu_c$, dimensionless
N'_{Re} = Reynolds number, $DV_s \rho_d/\mu_c$, dimensionless
$\overline{N}_{Re}$ = Reynolds number, $DV_o \rho_d/\mu_c$, dimensionless
n = fraction of collisions leading to coalescence, dimensionless
$\bar{n} = (wD/V_s)/\phi_d^{0.5}$, dimensionless
P = radius of disc, cm.
p = pressure, dynes/sq. cm.
Q = rate of removal of small drop by coalescence, sec.$^{-1}$
R = collision radius, cm.
r = radial coordinate
S = distance from center of gravity to plane $z = 0$, cm.
t = time, sec.; Student's test
t_C = time between collisions of a drop, sec.
$\overline{u(t)}$ = root mean square fluctuating velocity, cm./sec.
V = superficial velocity, cm./sec.; $-dH/dt$, cm./sec.
V_s = slip velocity, cm./sec.
v = velocity component, cm./sec.
w = coalescence frequency, sec.$^{-1}$
x, y, z = Cartesian coordinates
Δp = difference in pressure, dynes/sq. cm.

Greek Letters

$\Delta\rho$ = difference in density, g./cu. cm.
θ = angular coordinate
μ = viscosity, poises
ρ = density, g./cu. cm.
σ = interfacial tension, dynes/cm.
$\tau : \nabla \mathbf{v}$ = viscous dissipation, ergs/(cu. cm.)(sec.)
ϕ = volume fraction, dimensionless
$\psi = 1 - 2(S/D)$

Subscripts

c = continuous phase
d = dispersed phase
f = at end of deformation
i = transition between stages one and two
m = middle of deformation process
o = at the beginning
r = in the radial direction

LITERATURE CITED

1. Beyaert, B. O., Leon Lapidus, and J. C. Elgin, *AIChE J.*, **7**, 46 (1961).
2. Bird, R. B., W. E. Stewart, and E. N. Lightfoot, "Transport Phenomena," Wiley, New York (1960).
3. Boye-Christensen, G., and S. G. Terjersen, *Chem. Eng. Sci.*, **9**, 225 (1959).
4. Brown, A. H., *Chem. Ind. (London)*, **1968**, 990 (1968).
5. Charles, G. E., and S. G. Mason, *J. Colloid Sci.*, **15**, 236 (1960).
6. Damon, K. G., Ph.D. dissertation, Univ. Wisconsin, Madison (1967).
7. Dunn, I., Leon Lapidus, and J. C. Elgin, *AIChE J.*, **11**, 158 (1965).
8. Groothius, H., and F. J. Zuiderweg, *Chem. Eng. Sci.*, **19**, 63 (1964).
9. Hartland, S., *Trans. Inst. Chem. Engrs. (London)*, **45**, T97 (1967).
10. Hillestad, J. G., and J. H. Rushton, paper presented at AIChE meeting, Columbus, Ohio (May, 1966).
11. Howarth, W. J., *Chem. Eng. Sci.*, **19**, 33 (1964).
12. ———, *AIChE J.*, **13**, 1007 (1967).
13. Jeffreys, G. V., and J. L. Hawksley, *ibid.*, **11**, 413 (1965).
14. Lawson, G. B., *Chem. Process Eng.*, **48**, 45 (1967).
15. Letan, Ruth, and Ephraim Kehat, *AIChE J.*, **13**, 443 (1967).
16. Maraschino, M. J., Ph.D. dissertation, New York Univ., New York (1969).
17. Madden, A. J., and G. L. Damerell, *AIChE J.*, **8**, 233 (1962).
18. Miller, R. S., J. L. Ralph, R. L. Curl, and G. D. Towell, *ibid.*, **9**, 196 (1963).
19. Moreny, M. J., "Facts from Figures," pp. 286, 295, 311, Penguin Books, Baltimore (1956).
20. Schindler, H. D., and R. E. Treybal, *AIChE J.*, **14**, 790 (1968).
21. Treybal, R. E., "Liquid Extraction," 2nd edit., pp. 182–185, McGraw-Hill, New York (1963).

Manuscript received July 7, 1969; revision received October 7, 1969; paper accepted October 13, 1969. Paper presented at AIChE Atlanta meeting.